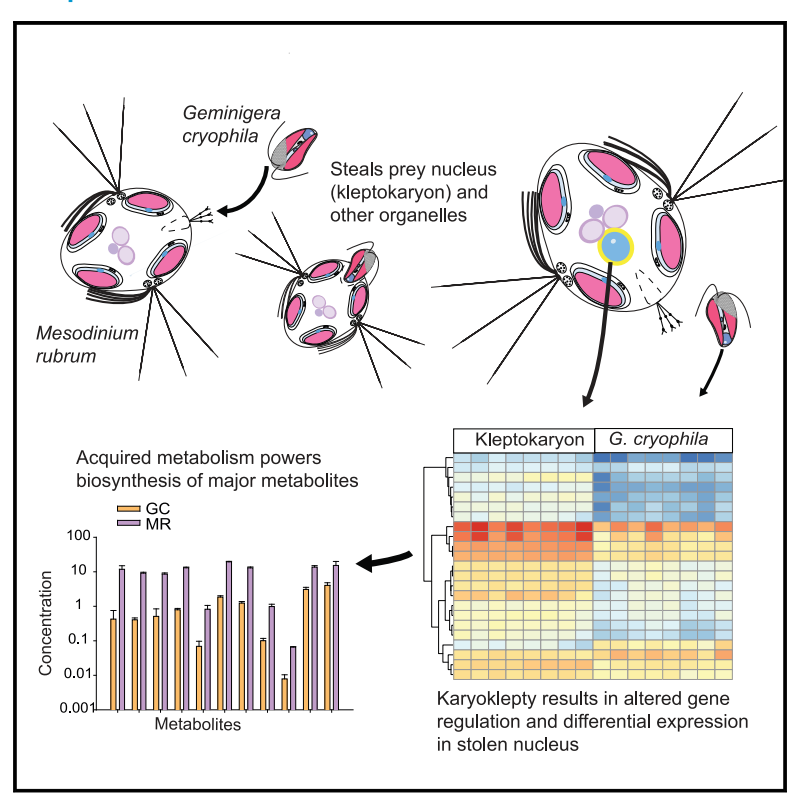
# Functional control and metabolic integration of stolen organelles in a photosynthetic ciliate

#### **Graphical abstract**



#### **Authors**

Matthew D. Johnson, Holly V. Moeller, Christopher Paight, Riss M. Kellogg, Matthew R. McIlvin, Mak A. Saito, Erica Lasek-Nesselquist

#### Correspondence

mattjohnson@whoi.edu

#### In brief

Johnson et al. show that the enslaved algal nucleus in *Mesodinium rubrum* is highly active transcriptionally but lacks fine-tuned regulation. Despite this, it retains the ability to regulate kleptoplastid pigment levels. Proteome and metabolome data reveal that the ciliate depends upon its stolen organelles for most of its biosynthetic needs.

#### **Highlights**

- M. rubrum steals prey nucleus (kleptokaryon) to acquire its metabolism
- M. rubrum remodels biosynthetic pathways of prey
- Kleptokaryon genes in M. rubrum lack fine-tuned regulation
- Ability to photoacclimate implies post-transcriptional regulation





#### Report

# Functional control and metabolic integration of stolen organelles in a photosynthetic ciliate

Matthew D. Johnson,<sup>1,5,\*</sup> Holly V. Moeller,<sup>2</sup> Christopher Paight,<sup>2</sup> Riss M. Kellogg,<sup>3</sup> Matthew R. McIlvin,<sup>3</sup> Mak A. Saito,<sup>3</sup> and Erica Lasek-Nesselquist<sup>4</sup>

<sup>1</sup>Biology Department, Woods Hole Oceanographic Institution, Woods Hole, MA 02543, USA

#### **SUMMARY**

Stealing prey plastids for metabolic gain is a common phenomenon among protists within aquatic ecosystems. Ciliates of the Mesodinium rubrum species complex are unique in that they also steal a transcriptionally active but non-dividing prey nucleus, the kleptokaryon, from certain cryptophytes.<sup>2</sup> The kleptokaryon enables full control and replication of kleptoplastids but has a half-life of about 10 days. Once the kleptokaryon is lost, the ciliate experiences a slow loss of photosynthetic metabolism and eventually death.<sup>2-4</sup> This transient ability to function phototrophically allows M. rubrum to form productive blooms in coastal waters.<sup>5-8</sup> Here, we show, using multi-omics approaches, that an Antarctic strain of the ciliate not only depends on stolen Geminigera cryophila organelles for photosynthesis but also for anabolic synthesis of fatty acids, amino acids, and other essential macromolecules. Transcription of diverse pathways was higher in the kleptokaryon than that in G. cryophila, and many increased in higher light. Proteins of major biosynthetic pathways were found in greater numbers in the kleptokaryon relative to M. rubrum, implying anabolic dependency on foreign metabolism. We show that despite losing transcriptional control of the kleptokaryon, M. rubrum regulates kleptoplastid pigments with changing light, implying an important role for post-transcriptional control. These findings demonstrate that the integration of foreign organelles and their gene and protein expression, energy metabolism, and anabolism occur in the absence of a stable endosymbiotic association. Our results shed light on potential events early in the process of complex plastid acquisition and broaden our understanding of symbiogenesis.

#### **RESULTS AND DISCUSSION**

For all analyses, we contrasted measurements between M. rubrum and its prey and source of organelles: the cryptophyte G. cryophila (Figure 1A). All measurements, except the metabolome, were taken during a photoacclimation experiment where cultures for both species were acclimated to high or low light, and then switched in a complementary manner to opposite conditions (Figure 1B) and monitored for chlorophyll a (chla) (Figure 1C), gene, and protein expression over time. Metabolomic measurements were taken at a steady state and intermediate light level between our high and low treatments. Changing light levels resulted in a photoacclimation response, where adjustments in chla cell<sup>-1</sup> occurred for both species, with M. rubrum requiring >1 week to reach a new acclimation state, while G. cryophila required ~5 days (Figure 1C). Differences in rate of change may be explained in part by differences in growth rate, which are  $\sim$ 50% higher for the cryptophyte.9

### Kleptokaryon transcriptome and regulatory responses to changing light

Previous research on *M. rubrum* has shown that roughly half of its global transcriptome is dominated by the kleptokaryon and that pathways involved in carbon, nitrogen, amino-acid (AA), and fatty-acid (FA)/lipid metabolism appear to be upregulated since they show higher normalized expression compared with their cryptophyte prey. While we did not analyze *M. rubrum* gene expression in detail, ~3.5× the number of genes were represented in the transcripts of free-living *G. cryophila* relative to the ciliate portion of the transcriptome (Data S1A). Overall the kleptokaryon represented 71.1% of the total genes recovered from the global *M. rubrum* transcriptome and 56.7% of unique Kyoto Encyclopedia of Genes and Genomes (KEGG) annotations (Data S1A).

The number of genes represented in transcripts in *G. cryophila* was 1.4× greater than in the kleptokaryon (Data S1A), indicating major transcriptional changes occur in the stolen nucleus. However, transcript expression levels for the kleptokaryon were



<sup>&</sup>lt;sup>2</sup>Department of Ecology, Evolution, and Marine Biology, University of California, Santa Barbara, Santa Barbara, CA 93106, USA

<sup>&</sup>lt;sup>3</sup>Department of Marine Chemistry and Geochemistry, Woods Hole Oceanographic Institution, Woods Hole, MA 02543, USA

<sup>&</sup>lt;sup>4</sup>New York State Department of Health (NYSDOH), Wadsworth Center, Albany, NY 12208, USA

<sup>&</sup>lt;sup>5</sup>Lead contact

<sup>\*</sup>Correspondence: mattjohnson@whoi.edu https://doi.org/10.1016/j.cub.2023.01.027



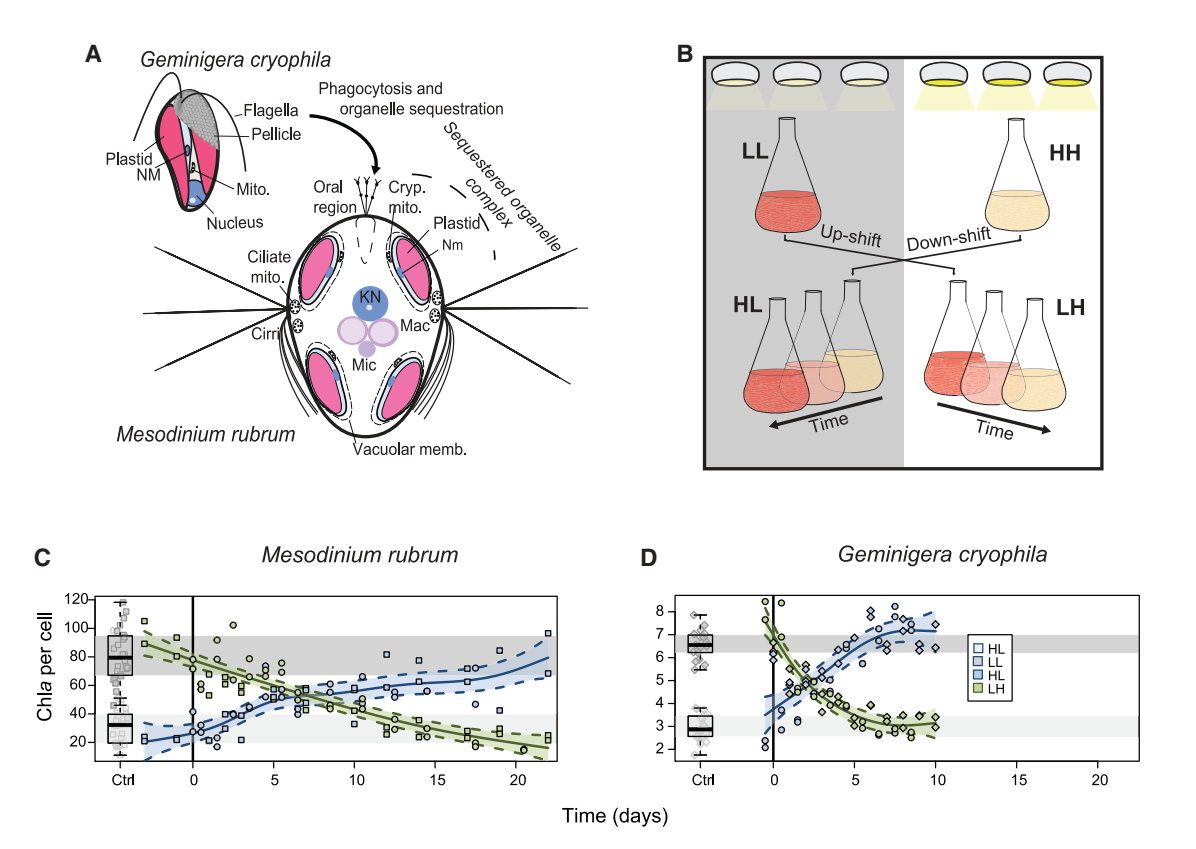


Figure 1. The model system of Mesodinium rubrum and Geminigera cryophila, experimental design of our photoacclimation experiments, and trends during experiments in cellular chlorophyll a (chla) during photoacclimation

(A) Cartoons of the ciliate Mesodinium rubrum and its prey (and source of foreign organelles), the cryptophyte G. cryophila. Figure illustrates some of the major features of M. rubrum and G. cryophila and highlights the organelles sequestered by the ciliate. KN, kleptokaryon (stolen nucleus); ciliate Mac, macro nucleus; ciliate Mic, micronucleus; mito, mitochondria; cryptophyte Nm, nucleomorph (reduced eukaryotic nucleus).

(B) The light-shift experimental design to assess photoacclimation in both cultures, with low-light (LL) acclimated cells shifted to high-light (LH), and high-light (HH) acclimated cells shifted to low light (HL).

(C and D) Plot of chla cell<sup>-1</sup> during photoacclimation response for M. rubrum (C) and G. cryophila (D). Shaded areas represent the interquartile range corresponding to box plots of the low-light (LL) and high-light (HH) controls. Scatter plots show replicates (n = 3) for each sample and the mean is plotted as a line with the 95% confidence interval enclosed in dashed lines and colored, green for low to high (LH) and blue for high to low (HL) treatments. Different data point shapes for (C) and (D) show data from replicated experiments, where only physiological parameters were measured. See also Table S4.

higher when normalized for gene length and sequencing depth for a number of key pathways involved in biosynthesis (e.g., AAs, FAs, porphyrin, and chlorophyll); energy (e.g., carbon fixation); catabolic organelles (e.g., lysosome and peroxisome); and metabolism (e.g., pentose phosphate pathway [PPP], tricarboxylic acid [TCA] cycle, and nitrogen metabolism) (Figure S1). In contrast, G. cryophila had higher levels of expression in only a few categories, including ribosome, DNA replication, cell growth, and calcium signaling (Figure S1).

Assessment of kleptokaryon pathway completeness, based on the number of nonredundant KEGG Orthology identifiers (KOs), averaged 90.8% (Table S1). Some of the most complete pathways (>95% by KO) for the kleptokaryon included AA biosynthesis, carbon fixation, carotenoid biosynthesis, porphyrin and chlorophyll metabolism, FA metabolism, nitrogen metabolism, the proteasome, and a variety of other metabolic and cellular functional pathways. Some of the most incomplete pathways (<80% by KO) included those related to cell growth, ribosome functioning, oxidative phosphorylation, and pathways that are associated with cell-information processing and replication and the cytoskeleton.

Our results clearly show that within G. cryophila, light-shift treatments successfully remodeled the transcriptome to resemble the new acclimation state. Principal components analysis (PCA) of G. cryophila transcriptome samples (biological replicates) revealed a clear separation of the light-shifted treatments from their original light levels, with high to low (HL) clustering closer to low-light (LL) and low to high (LH) clustering closer to high-light (HH) (Figure 2A). In contrast, the PCA plot for the kleptokaryon of M. rubrum revealed that biological replicates for light-shifted treatments were more similar to their original light level controls, indicating less global transcriptional change within the stolen nucleus in response to changing light and more change due to time (Figure 2B). Time appeared to be less of a factor in explaining relationships among G. cryophila samples. These results support the findings of Altenburger et al. 12 that most light-dependent transcriptional regulation of kleptokaryon genes is lost upon sequestration.



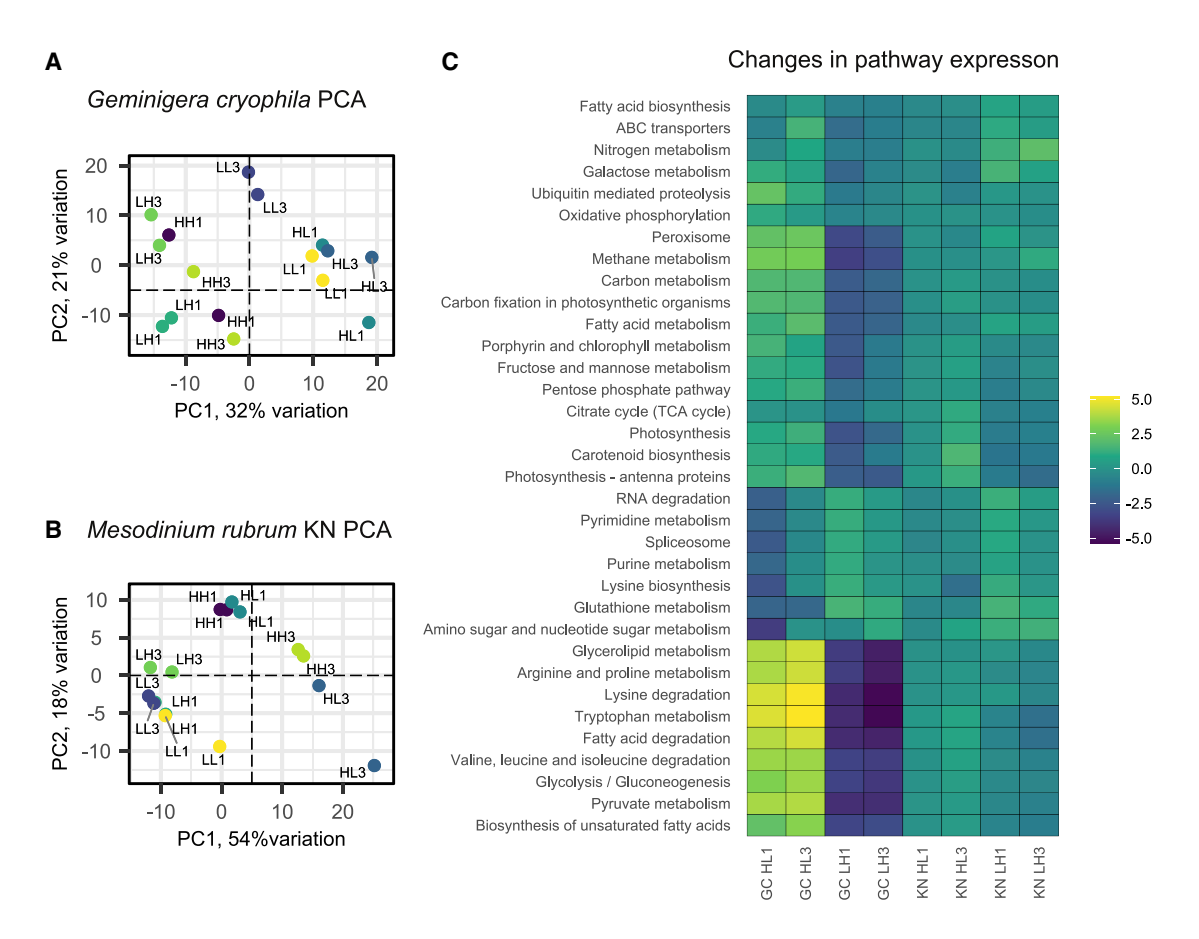


Figure 2. Principal component analysis (PCA) of all transcriptome samples of *Geminigera cryophila* and the kleptokaryon (KN) of *Mesodinium rubrum* and a heatmap depicting changes in average pathway expression levels for light treatments

(A and B) (A) PCA analysis of *G. cryophila* (top) and the (B) KN of *M. rubrum* (bottom), with sample triplicates depicted both by color and labeled.

(C) Heatmap of transcriptome treatment means for *G. cryophila* (GC) and the KN of *M. rubrum*, showing differential gene expression in major pathways relative to their light acclimation state of origin (see Figure 1B), for days 1 and 3. For all measurements n = 3.

See also Figures S1 and S2, Data S1A, and Table S1.

Patterns in higher-level expression changes for several KEGG-defined pathways were evaluated by averaging the fold-changes of differentially expressed genes. Most pathways showed a stronger response to shifts in light treatment for *G. cryophila* compared with the kleptokaryon in *M. rubrum*. In *G. cryophila*, some of the most differentially expressed pathways included AA metabolism, FA and lipid metabolism, and carbon metabolism. While changes in kleptokaryon transcription somewhat mirrored that of *G. cryophila* (Figure 2C), effects were more muted, reflecting overall higher expression levels in the kleptokaryon regardless of light intensity (see Figure S1).

## **Geminigera** and **Mesodinium** proteome characteristics and pathway comparisons

Across all samples, 15,780 and 33,749 unique (nonredundant) proteins were identified within *G. cryophila* and *M. rubrum* with a mean of 986 and 2,110 unique proteins discovered per sample, respectively (Table S2; Data S1B). This large number of unique proteins in *M. rubrum* reflects the complexity of the global *M. rubrum* proteome, which includes 4 eukaryotic and 3 organelle genomes, compared with 2 and 2, respectively, for

G. cryophila (Figure 1A). Of these proteins, 61% were annotated (with a GO term) in G. cryophila, while 69% were annotated in the kleptokaryon of M. rubrum and only 41% were annotated from the ciliate macronucleus (Data S1B). Overall  $\sim\!\!45\%$  of the total unique proteins in M. rubrum were from the kleptokaryon, while  $\sim\!\!56\%$  of annotated proteins were from the stolen nucleus.

Comparisons of proteome KO pathways between *G. cryophila*, the kleptokaryon, and the macronucleus of *M. rubrum* revealed a striking pattern of low protein numbers (Figure 3A) and lower count spectra (not shown) for ciliate macronuclear proteins involved in metabolism and anabolism. All pathways differed between the kleptokaryon and macronucleus of *M. rubrum* in the percent of total proteome proteins found, with all being higher in the former except for transcription, signaling and cellular processes, and unknown proteins (Figure 3B; Table S3). Similar to the transcriptome, the kleptokaryon had significantly more proteins related to carbohydrate, lipid, nucleotide, AA, co-factor and vitamin metabolism, and unclassified metabolism than *G. cryophila* (Figure 3A; Table S3). While *G. cryophila* and the *M. rubrum* macronucleus did not differ in protein expression for lipid and nucleotide pathways, significantly higher values were



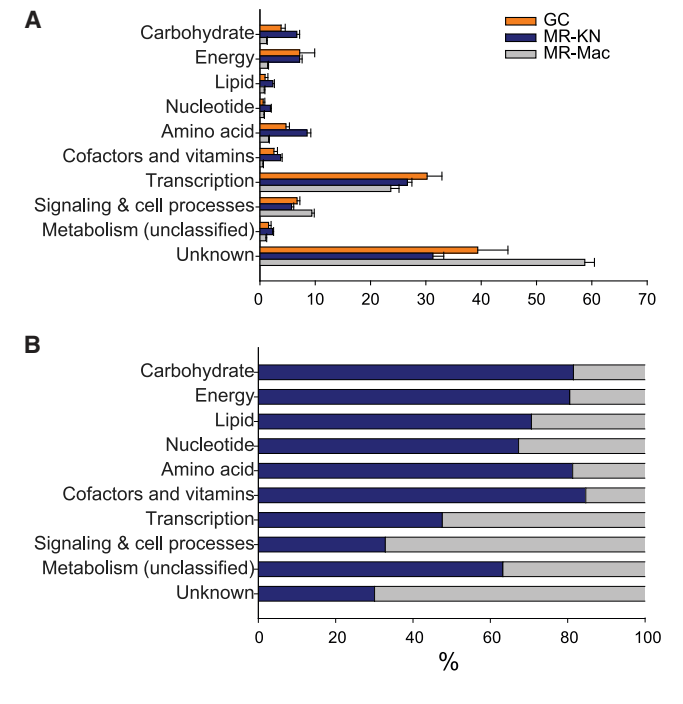


Figure 3. Proteome annotation for *Geminigera cryophila* (GC) and the kleptokaryon (KN) or macronucleus (Mac) of *Mesodinium rubrum* (MR)

(A) Percentage of unique proteins found in major pathways (annotated) or unknown in each proteome of GC, MR-KN, and the MR-Mac.

(B) Percent of global M. rubrum proteome pathways composed of KN or Mac proteins. For all measurements n=3. Error bars show standard deviation (p < 0.05).

See also Tables S2 and S3 and Data S1B.

found in the kleptokaryon compared with both (Table S3). Taken together, these results strongly suggest that the kleptokaryon of *M. rubrum* is responsible for fulfilling key metabolic and anabolic pathways, and its proteome is transformed to supplement lipid and AA biosynthesis of its host. These results demonstrate for the first time that the kleptokaryon in *M. rubrum* is not only highly transcriptionally active; it also produces an active and rich proteome to exploit its stolen cryptophyte organelles and their metabolism. These results also reveal the somewhat evolutionarily precarious nature of this relationship, since *M. rubrum* relies on the unstable kleptokaryon for numerous processes that appear to have either been lost or silenced in the ciliate (Figure 3).

## Physiological and metabolic control of cryptophyte biosynthetic pathways in *M. rubrum*

Photoacclimation is an intrinsic and essential mechanism of photosynthetic organisms to optimize light absorption, and orchestrating this response requires expression of numerous nuclear-encoded, plastid-targeted proteins. Photoacclimation does not occur in the majority of kleptoplastidic protists since they do not sequester the nucleus of their prey. In mixotrophic oligotrich ciliates, kleptoplastids have a short half-life (~1 day) and are rapidly turned over, <sup>13,14</sup> while *M. rubrum* can use the kleptokaryon from their prey to synthesize pigments, divide stolen organelles, and fully exploit their prey's metabolism. <sup>2,3,9–12,15</sup> We observed significant differences in chla cell<sup>-1</sup> with time and

light exposure (Table S4) and an overall slower photoacclimation response in *M. rubrum* compared with *G. cryophila* (Figures 1C and 1D).

The transcriptional dynamics of the kleptokaryon contrasted starkly with the fine-tuned light-driven response of cryptophyte metabolism (Figures 2C and S1). Gene-expression responses varied greatly between G. cryophila and the kleptokaryon when evaluated individually within pathways. Nearly all genes involved in the TCA cycle were upregulated in G. cryophila regardless of light treatment, particularly in HL (Figure S2A). In contrast, the kleptokaryon revealed treatment-specific responses with upregulation in LH and downregulation in HL. In G. cryophila, PPP (not shown) and glycolysis (Figure S2B) gene expression were upregulated in HL and downregulated in LH, while in the kleptokaryon the pattern was reversed. For photosynthesis, the same general pattern was found in G. cryophila as observed with PPP, while kleptokaryon expression showed no pattern (Figure S2C). In general, FA pathways were more broadly represented in the kleptokaryon transcriptomes relative to G. cryophila, suggesting functional changes to cryptophyte lipid metabolism in M. rubrum or enrichment of gene expression from this pathway relative to global transcription (Figure S2D). As with other metabolic pathways, FA biosynthesis in the kleptokaryon was upregulated with increased light, while the opposite was true for G. cryophila. The stimulation of transcription within the kleptokaryon by light suggests that some regulation of kleptokaryon genes is retained in M. rubrum for pathways involved in carbon metabolism and energy. As previously suggested, 10 this response may simply reflect enhanced metabolic feedback on kleptokaryon transcriptional control driven by a higher plastid-to-nucleus ratio ( $\sim$ 10) and an overabundance of substrate from light-saturated photosynthesis.

Previous research on the same strain of M. rubrum revealed that macromolecule metabolic pools fed from carbon fixation differ slightly from G. cryophila in having a greater proportion of photosynthate entering lipid metabolism.9 Steady-state AA and FA transcriptome and proteome expression data were compared with metabolomic data for these pathways between G. cryophila and the kleptokaryon of M. rubrum (Figure S3). While the precise source of metabolites for M. rubrum is difficult to interpret as it represents some mixture of the kleptokaryonand ciliate-encoded metabolism, proteome data for both lipids and AA clearly show greater contributions by the kleptokaryon. For AAs, gene expression was clearly greater at LL for G. cryophila and in HH for the kleptokaryon (Figures S3A and S3B). Protein expression for G. cryophila was variable, but greater proportions of peptides were higher in HH, while nearly all kleptokaryon peptide expression was distinctly higher in HH (Figure S3B). Not surprisingly, metabolomic data revealed consistently greater concentrations of cell-normalized AA concentrations in M. rubrum, with all but aspartic acid being >10× the level of G. cryophila (Figure 4A). Most starkly, however, levels of tryptophan and glutamine were 100× and 75× greater, respectively, in M. rubrum (Figure 4A), implicating a key role for these molecules in other metabolic pathways.

The production of AA within *M. rubrum* appeared to be powered largely by the high levels of transcription and protein expression observed within the kleptokaryon. This conclusion is supported by low protein expression and underrepresented



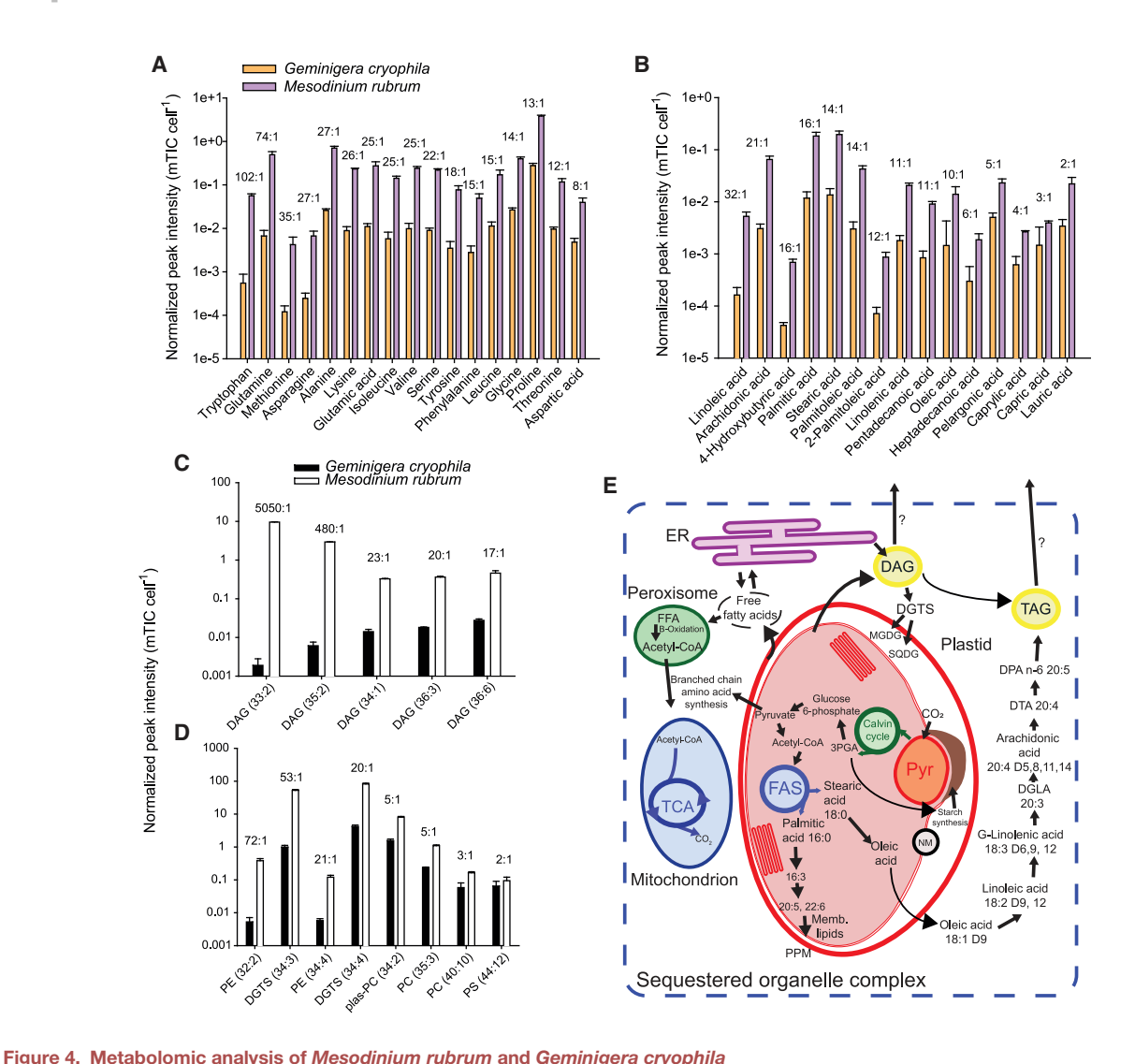


Figure 4. Metabolomic analysis of *Mesodinium rubrum* and *Geminigera cryopnila* 

(A–D) Metabolomic data for (A) amino acids, (B) fatty acids, (C) diacylglycerols (DAGs), and (D) select lipids in *M. rubrum* and *G. cryophila*. Metabolomic data are shown as normalized peak intensity per cell, with the MR:GC ratio shown above each pair of metabolite columns.

(E) Cartoon of hypothetical pathways for fatty acid, DAG, triacylglycerol (TAG), and lipid biosynthesis in the organelle complexes of *M. rubrum*. Dashed line in (C) represents the membrane around the plastid-mitochondrial complex (PMC). Ratios next to compound names are the number of carbon atoms to number of saturated bonds, while ratios above inset bar graphs show the MR:GC ratio of each compound. Question marks illustrate the unknown fate of major FA pools with the ciliate cytoplasm. FAS, fatty acid synthesis; Pyr, pyrenoid; NM, nucleomorph; PPM, periplastidal membrane; PGA, phosphoglycerate; DGLA, dihomoγ-linolenic acid; DTA, docosatetraenoic acid; DPA, docosapentaenoic acid; DGTS, diacylglyceryltrimethylhomo-Ser; MGDG, monogalactosyldiacylglycerol; SQDG, sulfoquinovosyl-diacylglycerol. For all metabolomic measurements, n = 6. Error bars show standard deviation (p < 0.05). See also Figure S3.

pathways for AA in the ciliate in this study and is consistent with analysis of another *M. rubrum* variant, which showed a reliance upon the stolen nucleus for lysine synthesis and overall enhanced AA transcription. The transcription of AA genes within the kleptokaryon and *G. cryophila* had opposite regulation patterns in response to light acclimation level, but the effect was lost in the proteome where expression for both increased in high light. The higher expression of AA genes and proteins by the kleptokaryon of *M. rubrum* relative to free-living *G. cryophila* was consistent with greater levels of AA within the *M. rubrum* metabolome, which were on average 2.8× higher than in *G. cryophila* after normalizing to cell carbon. The high levels of

glutamine in *M. rubrum* were not surprising, considering it is central to numerous biosynthetic pathways. However, the very high levels of tryptophan relative to *G. cryophila* suggest that it may have additional roles in the ciliate. In a study comparing AA levels of two ciliates with their cryptophyte prey, tryptophan was also found to be present at significantly higher levels in the ciliates <sup>16</sup> and is known to be a key component in pheromones of the heterotrich ciliate *Blepharisma*. <sup>17</sup>

For FA gene transcription, levels were similar between LL and HH treatments of *G. cryophila*, falling along a 1:1 line, but were higher in the HH treatment for the kleptokaryon (Figure S3C). Protein levels, however, were clearly higher in the LL treatment



Current Biology Report

of G. cryophila and in the HH treatment of M. rubrum (Figure S3D). Metabolomic data revealed FA levels that were 3-to-32× higher for all compounds in M. rubrum (Figure 4B). The disparity was even greater, however, when comparing diacylglycerols (DAGs), which were ~500 and 5,000× more abundant in M. rubrum (Figure 4C). The phospholipids phosphatidylethanolamine (PE), phosphatidylserine (PS), and phosphatidylcholine (PC) and the betaine lipid 1,2-diacylglyceryl-3-O-4'-(N,N,N-trimethyl)-homoserine (DGTS) were also characterized from these samples (Figure 4D). While all lipids were more abundant in M. rubrum, PC and PS were found at proportionally higher levels (i.e., normalized to cell carbon) in G. cryophila (Figure 4D) when considering that the ciliate has  $\sim 10 \times$  the biomass. 14 A conceptual diagram of the cryptophyte sequestered organelle complex within M. rubrum and its potential FA and lipid metabolic pathways, based on observed metabolomic data (Figure 4E), highlights its robust potential for powering these biosynthetic pathways in the ciliate. While we found high expression of kleptokaryon peroxisome-targeted genes in our M. rubrum samples and include this organelle in our conceptual diagram (Figure 4E), we have no direct evidence to indicate its role in the ciliate.

In G. cryophila, transcription within FA biosynthetic pathways terminated in production of stearoyl-CoA (C18) and palmitoyl-CoA (C16) and lacked expression of genes involved in verylong-chain FA pathways. Our metabolomic analysis revealed a variety of polyunsaturated FA in G. cryophila and M. rubrum, originating from plastid biosynthetic pathways. These results were consistent with previous research demonstrating that cryptophytes produce a variety of long-chain polyunsaturated omega-3 FA, including  $\alpha$ -linolenic acid (18:3: $\omega$ 3), stearidonic acid (18:4ω3), eicosapentaenoic acid (20:5:ω3), and docosahexaenoic acid (22:6:ω3).18 However, gene expression of FA pathways within the kleptokaryon of M. rubrum were much more extensive and revealed complete pathways of very-long-chain FA (C28), including very-long-chain enoyl-CoA and very-longchain (3R)-3-hydroxyacyl-CoA dehydratase, which is responsible for extending palmitoyl-CoA and stearoyl-CoA. The production of very long FA gene pathways in M. rubrum grown in high light suggest that FA biosynthesis may also be used to synthesize DAGs and accumulate stores of triacylglycerols (TAGs), both of which occurred at much greater concentrations in M. rubrum.

#### **Evolutionary implications**

The origin of modern eukaryotic plastid diversity has involved multiple secondary and tertiary symbiotic acquisitions from red and green plastid lineages. While the exact number of events has been debated, <sup>19,20</sup> it is now apparent that stable plastid acquisitions are not as rare as once thought. As members of the alveolates, ciliates were once thought to have a photosynthetic ancestry and have even been shown to possess a small number of genes that appear to have algal origins. <sup>21</sup> However, no plastid-targeted genes have been found in ciliates, nor has any evidence for a vestigial plastid. In contrast, kleptoplastidic dinoflagellates have been shown to retain genes involved in plastid function and metabolism, which in certain cases appear to facilitate the exploitation of stolen plastids. <sup>22</sup> These dramatic differences in photosynthetic function and ancestry found between ciliates and dinoflagellates provide unique perspectives for

understanding adaptations to exploiting photosynthesis when investigating extant organelle-stealing species.

Despite weak evidence for a recent photosynthetic ancestry or the possession of genes that would mechanistically facilitate kleptoplasty, many ciliates are quite adept at hosting plastids and exploiting photosynthetic metabolism. Here we have shown that, by also enslaving a functional prey nucleus, *M. rubrum* is able to regulate its plastid pigment levels, remodel protein expression for metabolic pathways, and exploit the biosynthetic machinery of its prey for AA and FA pathways. While the expression levels for many kleptokaryon pathways are upregulated and appear to be driven higher by light, normal light-mediated transcriptional regulatory patterns found in *G. cryophila* are clearly lost in *M. rubrum*.

While stable plastid acquisitions are traditionally considered to be the product of endosymbiotic associations, there is growing acceptance that organelle sequestration may be a more relevant model for cellular and metabolic adaptation to phototrophy when acquiring complex plastids. <sup>23,24</sup> Organisms that steal a prey nucleus are particularly interesting since they are subject to selective pressure for evolving mechanisms to orchestrate *de novo* transcription and protein-targeting mechanisms. Whether or not karyoklepty also functions as a ratchet for facilitating "endosymbiotic" gene transfer, <sup>25</sup> however, remains unclear. In *M. rubrum*, selective pressure has dramatically transformed the ciliate into an organelle-stealing specialist, which is reliant upon the metabolism and anabolism of its prey and caught in a Promethean struggle of perpetually needing to reacquire the kleptokaryon.

#### **STAR**\*METHODS

Detailed methods are provided in the online version of this paper and include the following:

- KEY RESOURCES TABLE
- RESOURCE AVAILABILITY
  - Lead contact
  - Materials Availability
  - Data and code availability
- EXPERIMENTAL MODEL AND SUBJECT DETAILS
  - Mesodinium rubrum and Geminigera cryophila maintenance
- METHOD DETAILS
  - Experimental design and sampling
  - Cell counts, chlorophyll, and photophysiological measurements
  - Transcriptomics
  - Proteomics
  - Metabolomics
- QUANTIFICATION AND STATISTICAL ANALYSIS

#### SUPPLEMENTAL INFORMATION

Supplemental information can be found online at https://doi.org/10.1016/j.cub.2023.01.027.

#### **ACKNOWLEDGMENTS**

M.D.J. and H.V.M. would like to thank David Beaudoin, and M.A.S. would like to thank Dawn Moran for their assistance in the lab. We thank Kelly Paglia and

#### Report



Oliver Fiehn of the West Coast Metabolomics Center for their assistance with the metabolomic data. M.D.J. acknowledges the funding support of NSF IOS award 1354773. H.V.M. acknowledges funding from an NSF Postdoctoral Research Fellowship in Biology. Research was also sponsored by the U.S. Army Research Office and accomplished under contract W911NF-19-D-0001 for the Institute for Collaborative Biotechnologies.

#### **AUTHOR CONTRIBUTIONS**

M.D.J. and E.L.-N. conceived of the study. M.D.J., E.L.-N., H.V.M., C.P., and M.A.S. developed the methodology. H.V.M. performed and sampled all experiments, and M.R.M. and R.M.K. performed in-house proteomic sample extraction and analysis. E.L.-N., C.P., and M.D.J. analyzed the transcriptome data. M.R.M., M.A.S., C.P., E.L.-N., and M.D.J. analyzed the proteome data. M.D.J. analyzed the metabolomic data. M.D.J. drafted the manuscript and all authors helped to edit it.

#### **DECLARATION OF INTERESTS**

The authors declare no competing interests.

Received: September 27, 2022 Revised: November 15, 2022 Accepted: January 16, 2023 Published: February 10, 2023

#### **REFERENCES**

- Stoecker, D.K., Johnson, M.D., deVargas, C., and Not, F. (2009). Acquired phototrophy in aquatic protists. Aquat. Microb. Ecol. 57, 279–310.
- Johnson, M.D., Oldach, D., Delwiche, C.F., and Stoecker, D.K. (2007). Retention of transcriptionally active cryptophyte nuclei by the ciliate Myrionecta rubra. Nature 445, 426–428.
- Gustafson, D.E., Stoecker, D.K., Johnson, M.D., Van Heukelem, W.F., and Sneider, K. (2000). Cryptophyte algae are robbed of their organelles by the marine ciliate *Mesodinium rubrum*. Nature 405, 1049–1052.
- Kim, M., Drumm, K., Daugbjerg, N., and Hansen, P.J. (2017). Dynamics of sequestered cryptophyte nuclei in *Mesodinium rubrum* during starvation and refeeding. Front. Microbiol. 8, 423.
- Herfort, L., Peterson, T.D., McCue, L.A., Crump, B.C., Prahl, F.G., Baptista, A.M., Campbell, V., Warnick, R., Selby, M., Roegner, G.C., et al. (2011). *Myrionecta rubra* population genetic diversity and its cryptophyte chloroplast specificity in recurrent red tides in the Columbia River Estuary. Aquat. Microb. Ecol. 62, 85–97.
- Taylor, F.J.R., Blackbourn, D.J., and Blackbourn, J. (1971). The red-water ciliate *Mesodinium rubrum* and its "incomplete symbionts": a review including new ultrastructural observations. J. Fish. Res. Bd. Can. 28, 391–407.
- Lindholm, T. (1985). Mesodinium rubrum—a unique photosynthetic ciliate. Adv. Aquat. Microbiol 3, 1–48.
- Crawford, D.W. (1989). Mesodinium rubrum: the phytoplankter that wasn't. Mar. Ecol. Prog. Ser. 58, 161–174.
- Johnson, M.D., Tengs, T., Oldach, D., and Stoecker, D.K. (2006).
   Sequestration, performance, and functional control of cryptophyte plastids in the ciliate *Myrionecta rubra* (Ciliophora) 1. J. Phycol. 42, 1235–1246.
- Lasek-Nesselquist, E., Wisecaver, J.H., Hackett, J.D., and Johnson, M.D. (2015). Insights into transcriptional changes that accompany organelle sequestration from the stolen nucleus of *Mesodinium rubrum*. BMC Genom. 16, 805.
- Kim, G.H., Han, J.H., Kim, B., Han, J.W., Nam, S.W., Shin, W., Park, J.W., and Yih, W. (2016). Cryptophyte gene regulation in the kleptoplastidic, karyokleptic ciliate Mesodinium rubrum. Harmful Algae 52, 23–33.
- Altenburger, A., Cai, H., Li, Q., Drumm, K., Kim, M., Zhu, Y., Garcia-Cuetos, L., Zhan, X., Hansen, P.J., John, U., et al. (2021). Limits to the cellular control of sequestered cryptophyte prey in the marine ciliate *Mesodinium rubrum*. ISME J. 15, 1056–1072.

- Stoecker, D.K., and Silver, M.W. (1990). Replacement and aging of chloroplasts in Strombidium capitatum (Ciliophora: Oligotrichida). Mar. Biol. 107, 491–502.
- Schoener, D.M., and McManus, G.B. (2012). Plastid retention, use, and replacement in a kleptoplastidic ciliate. Aquat. Microb. Ecol. 67, 177–187.
- Johnson, M.D., and Stoecker, D.K. (2005). Role of feeding in growth and photophysiology of *Myrionecta rubra*. Aquat. Microb. Ecol. 39, 303–312.
- Boëchat, I.G., and Adrian, R. (2005). Biochemical composition of algivorous freshwater ciliates: you are not what you eat. FEMS Microbiol. Ecol. 53, 393–400.
- Sugiura, M., Yuasa, H.J., and Harumoto, T. (2017). Novel specificity of IDO enzyme involved in the biosynthesis of mating pheromone in the ciliate Blepharisma stoltei. Protist 168, 686–696.
- 18. Peltomaa, E., Johnson, M.D., and Taipale, S.J. (2017). Marine cryptophytes are great sources of EPA and DHA. Mar. Drugs 16, 3.
- Keeling, P.J. (2010). The endosymbiotic origin, diversification and fate of plastids. Philos. Trans. R. Soc. Lond. B Biol. Sci. 365, 729–748.
- Archibald, J.M. (2015). Endosymbiosis and eukaryotic cell evolution. Curr. Biol. 25, R911–R921.
- Reyes-Prieto, A., Moustafa, A., and Bhattacharya, D. (2008). Multiple genes of apparent algal origin suggest ciliates may once have been photosynthetic. Curr. Biol. 18, 956–962.
- 22. Wisecaver, J.H., and Hackett, J.D. (2010). Transcriptome analysis reveals nuclear-encoded proteins for the maintenance of temporary plastids in the dinoflagellate *Dinophysis acuminata*. BMC Genom. 11, 366.
- 23. Johnson, M.D. (2011). The acquisition of phototrophy: adaptive strategies of hosting endosymbionts and organelles. Photosynth. Res. 107, 117–132.
- Bodył, A. (2018). Did some red alga-derived plastids evolve via kleptoplastidy? A hypothesis. Biol. Rev. Camb. Philos. Soc. 93, 201–222.
- Doolittle, W.F. (1998). You are what you eat: a gene transfer ratchet could account for bacterial genes in eukaryotic nuclear genomes. Trends Genet. 14, 307–311.
- Team, R.C. (2013). R: A Language and Environment for Statistical Computing (R Foundation for Statistical Computing).
- Love, M.I., Huber, W., and Anders, S. (2014). Moderated estimation of fold change and dispersion for RNA-seq data with DESeq2. Genome Biol. 15, 550.
- Haas, B.J., Papanicolaou, A., Yassour, M., Grabherr, M., Blood, P.D., Bowden, J., Couger, M.B., Eccles, D., Li, B., Lieber, M., et al. (2013). De novo transcript sequence reconstruction from RNA-seq using the Trinity platform for reference generation and analysis. Nat. Protoc. 8, 1494–1512.
- Altschul, S.F., Gish, W., Miller, W., Myers, E.W., and Lipman, D.J. (1990).
   Basic local alignment search tool. J. Mol. Biol. 215, 403–410.
- Altschul, S.F., Madden, T.L., Schäffer, A.A., Zhang, J., Zhang, Z., Miller, W., and Lipman, D.J. (1997). Gapped BLAST and PSI-BLAST: a new generation of protein database search programs. Nucl. Acids Res. 25, 3389–3402.
- Camacho, C., Coulouris, G., Avagyan, V., Ma, N., Papadopoulos, J., Bealer, K., and Madden, T.L. (2009). Blast+: architecture and applications. BMC Bioinform. 10, 421.
- 32. Li, H., and Durbin, R. (2009). Fast and accurate short read alignment with Burrows–Wheeler transform. Bioinformatics 25, 1754–1760.
- Quinlan, A.R., and Hall, I.M. (2010). BEDTools: a flexible suite of utilities for comparing genomic features. Bioinformatics 26, 841–842.
- Kind, T., Liu, K.H., Lee, D.Y., DeFelice, B., Meissen, J.K., and Fiehn, O. (2013). LipidBlast in silico tandem mass spectrometry database for lipid identification. Nat. Methods 10, 755–758.
- Guillard, R.R. (1975). Culture of phytoplankton for feeding marine invertebrates. In Culture of Marine Invertebrate Animals (Springer), pp. 29–60.
- Sambrook, J., Fritsch, E.F., and Maniatis, T. (1989). Molecular Cloning: a Laboratory Manual, Second Edition (Cold Spring Harbor Laboratory Press).



- 37. Kanehisa, M., Sato, Y., Furumichi, M., Morishima, K., and Tanabe, M. (2019). New approach for understanding genome variations in KEGG. Nucl. Acids Res. 47, D590-D595.
- 38. Hughes, C.S., Foehr, S., Garfield, D.A., Furlong, E.E., Steinmetz, L.M., and Krijgsveld, J. (2014). Ultrasensitive proteome analysis using paramagnetic bead technology. Mol. Syst. Biol. 10, 757.
- 39. Perez-Riverol, Y., Bai, J., Bandla, C., García-Seisdedos, D., Hewapathirana, S., Kamatchinathan, S., Kundu, D.J., Prakash, A., Frericks-Zipper, A., Eisenacher, M., et al. (2022). The PRIDE database resources in 2022: a hub for mass spectrometry-based proteomics evidences. Nucleic Acids Res. 50, D543-D552.
- 40. Lee, D.Y., Park, J.J., Barupal, D.K., and Fiehn, O. (2012). System response of metabolic networks in Chlamydomonas reinhardtii to total available ammonium. Mol. Cell. Proteomics 11, 973-988.
- 41. Lai, Z., Tsugawa, H., Wohlgemuth, G., Mehta, S., Mueller, M., Zheng, Y., Ogiwara, A., Meissen, J., Showalter, M., Takeuchi, K., et al. (2018). Identifying metabolites by integrating metabolome databases with mass spectrometry cheminformatics. Nat. Methods 15, 53-56.
- 42. Matyash, V., Liebisch, G., Kurzchalia, T.V., Shevchenko, A., and Schwudke, D. (2008). Lipid extraction by methyl-tert-butyl ether for highthroughput lipidomics. J. Lip. Res. 49, 1137-1146.

# **Current Biology** Report



#### **STAR**\***METHODS**

#### **KEY RESOURCES TABLE**

REAGENT or RESOURCE	SOURCE	IDENTIFIER
Chemicals, peptides, and recombinant proteins		
Trizol	Thermo Fisher Scientific	15596026
HEPES	Thermo Fisher Scientific	15630106
SDS	Thermo Fisher Scientific	28364
Benzonase nuclease	Sigma Aldrich	E1014
OTT (dithiothreitol)	Thermo Fisher Scientific	R0861
odoacetamide	Sigma Aldrich	l1149
ormic acid	Sigma Aldrich	F0507
acetonitrile	Sigma Aldrich	271004
ethanol	Sigma Aldrich	E7023
Trypsin	Promega	VA9000
Frifluoroacetic acid	Sigma Aldrich	80457
DMSO	Sigma Aldrich	D2650
methyl tert-butyl ether	Sigma Aldrich	650560
ammonium formate	Sigma Aldrich	70221
Methanol	Sigma Aldrich	34860
oluene	Sigma Aldrich	650579
nethoxyamine hydrochloride	Sigma Aldrich	89803
Pyridine	Sigma Aldrich	270407
MSTFA	Sigma Aldrich	69479
Critical commercial assays		
KAPA-stranded RNA-Seq kit	Roche	KK8400
/ivaspin 5K MWCO ultrafiltration units	Sartorius	VS2011
SpeedBead Magnetic Carboxylate Modified Particles	Sigma Aldrich	GE17152104010150
Micro BCA Protein Assay Kit	Sigma Aldrich	71285
Deposited data		
Proteome data	this study	ProteomeXchange (PXD035728)
ranscriptome data	this study	www.ncbi.nlm.nih.gov/bioproject/PRJNA560206
Experimental models: Organisms/strains		
Mesodinium rubrum CCMP/NCMA 2563	NCMA	2563
Geminigera cryophila CCMP/NCMA 2564	NCMA	2564
Software and algorithms	NOMA	2304
Adobe	Illustrator	www.adobe.com/products/illustrator.html
Systat Software	Sigma Plot	systatsoftware.com/sigmaplot/
R Studio, Version 4.1.1	Team R <sup>26</sup>	www.r-project.org/
DESeq2	Love et al. <sup>27</sup>	bioconductor.org/packages/release/bioc/html/
DEGEQ2	Love et al.	DESeq2.html
PCAtools	N/A	github.com/kevinblighe/PCAtools
Oplyr, Version 1.0.7	N/A	dplyr.tidyverse.org/news/index.html
ggpubr, Version 0.4.0	N/A	cloud.r-project.org/web/packages/ggpubr/index.html
qqplotr, Version 0.0.5	N/A	cran.r-project.org/web/packages/qqplotr/index.html
pplots, Version 3.1.1	N/A	cran.r-project.org/web/packages/gplots/index.html
ggplot2, Version 3.3.5	N/A	cran.r-project.org/web/packages/ggplot2/index.html
:=:		(Continued on next pa

(Continued on next page)





Continued		
REAGENT or RESOURCE	SOURCE	IDENTIFIER
Rcompanion, Version 2.4.6	N/A	cran.r-project.org/web/packages/rcompanion/index. html
coin, Version 1.4-2	N/A	cran.r-project.org/web/packages/coin/index.html
FSA, Version 0.9.1	N/A	cran.r-project.org/web/packages/FSA/index.html
Lattice, Version 0.20-45	N/A	cran.r-project.org/web/packages/lattice/index.html
Trinity, Version 2.2.0	Haas et al. <sup>28</sup>	github.com/trinityrnaseq/trinityrnaseq/releases
BBMap, Version 35.82	N/A	sourceforge.net/projects/bbmap/
TransDecoder, Version 5.5.0	N/A	github.com/TransDecoder/TransDecoder
BLASTp, Version 2.9.0	Altschul et al. <sup>29,30</sup> and Camacho et al. <sup>31</sup>	blast.ncbi.nlm.nih.gov
BWA, Version 0.7.17	Li et al. <sup>32</sup>	guix.gnu.org/packages/bwa-0.7.17/
BEDTools, Version 2.28.0	Quinlan et al. <sup>33</sup>	bedtools.readthedocs.io/en/latest/
Proteome Discoverer	Thermo Fisher Scientific	N/A
Scaffold, Version 5.1.2	Promega	N/A
ChemStation	Agilent	N/A
FIREPRO, Version 1.20	N/A	www.firefluorometers.com/
Maestro Gerstel software, Version 1.1.4.18	Gerstel	N/A
Leco ChromaTOF software, Version 2.32	Leco	N/A
MassHunter Software	Agilent	N/A
LipidBlast	Kind et al. <sup>34</sup>	fiehnlab.ucdavis.edu/projects/lipidblast/

#### **RESOURCE AVAILABILITY**

#### **Lead contact**

Further information and requests for resources and data should be directed to the lead contact, Matthew Johnson (mattjohnson@ whoi.edu).

#### **Materials Availability**

This study did not generate new or unique reagents or materials.

#### **Data and code availability**

- Original transcriptomic and proteomic data have been deposited and have been made publicly available prior to publication (see key resources table). Metabolomic and pigment data are available upon request to the corresponding author.
- All code used for transcriptomic data analyses are available here.
- Any additional information required to reanalyze the data reported in this paper is available from the lead contact upon request.

#### **EXPERIMENTAL MODEL AND SUBJECT DETAILS**

#### Mesodinium rubrum and Geminigera cryophila maintenance

Cultures of the ciliate Mesodinium rubrum (CCMP 2563) and its cryptophyte prey, Geminigera cryophila (CCMP 2564), were originally isolated from McMurdo Sound, Antarctica. Batch cultures of M. rubrum and G. cryophila were routinely maintained in F/2-Si media. that was 0.2 µm filtered and autoclaved using 35 PSU seawater from Martha's Vineyard Sound, and maintained at 4 °C under 24h fluorescent white light. M. rubrum cultures were fed G. cryophila at a prey: predator ratio of  $\sim$ 5:1 when transferred, once every 2 weeks. Cultures for all experiments (n = 3) except the metabolomics were acclimated to either low (5 μmol photons m<sup>-2</sup> s<sup>-1</sup>) or high (65 μmol photons m<sup>-2</sup> s<sup>-1</sup>) irradiance levels for ten months prior to the start of the experiment. During this time M. rubrum was fed G. cryophila from the same acclimation light level. These light levels were chosen based on previous research on the steady photoacclimation states of M. rubrum to a broad array of irradiance levels. 14 A custom tunable LED white light array was used to achieve desired light levels. Mesodinium cultures were last fed with G. cryophila 4 days prior to our experimental time 0 sampling point. Cultures for the metabolomics measurements (n = 6) were grown under identical conditions to our routine maintenance above, but at 30 μmol photons m<sup>-2</sup> s<sup>-1</sup>.

Report



#### **METHOD DETAILS**

#### **Experimental design and sampling**

For the photoacclimation experiment, a complementary design was employed where both M. rubrum and G. cryophila cultures were kept at their respective acclimation irradiances or switched to the other light level. Switching between low to high light (LH) and high to low light (HL) represented the experimental acclimation treatments and are referred to as "light-shift" treatments. Cultures that remained at their acclimation state, in low light (LL) and high light (HH), served as controls (Figure 1B). All flasks were 4L, with approximately 3.5L of culture media at T0. Cultures of M. rubrum were sampled daily for the first 8 days of the experiment, and then every other day thereafter for a total 20 days. G. cryophila cultures were sampled daily for 12 days.

#### Cell counts, chlorophyll, and photophysiological measurements

Cells were preserved with 5% acid Lugol's solution (5% I, 10% KI, 10% acetic acid) at each time point and stored at room temperature until counted using a Sedwick Rafter (M. rubrum) or hemocytometer (G. cryophila) counting chamber and a Zeiss Axiophont microscope. Chlorophyll a was determined by filtering 5-25 mL of culture onto a Whatman GF/F filter and extracting overnight in 90% acetone at -20°C, and the resulting sample was measured with a TD-700 (Turner Designs, Sunnyvale, CA) fluorometer.

#### **Transcriptomics**

#### RNA extraction and RNA-Seq library preparation

Cells were harvested on days 1 and 3 for both ciliate and cryptophyte cultures. To collect cell material for RNA extractions, M. rubrum cultures were gently filtered on 1 µm polycarbonate filters and flash frozen in liquid nitrogen for later analysis.

RNA was extracted from frozen pellets using a standard Trizol procedure.36 Poly-A enriched libraries were generated with the KAPA-stranded RNA-Seq kit and 150-bp paired-end sequencing was performed on an Illumina HiSeq 4000 at the University of Georgia Genomics Genome Facility. All treatments had two biological replicates.

#### Transcriptome analysis

Mesodinium rubrum and Geminigera cryophila transcriptomes were assembled de novo with Trinity v.2.2.0<sup>28</sup> after removing adaptors and low-quality reads with BBDuk from BBMap v.35.82 (https://sourceforge.net/projects/bbmap/; last accessed November 4, 2019). Proteins were predicted by TransDecoder v.5.5.0 with the Mesodinium genetic code option for M. rubrum libraries or the standard genetic code for G. cryophila libraries (https://github.com/TransDecoder; last accessed November 4, 2019). Proteins were submitted to the KEGG server for KEGG orthology (KO) annotation and pathway assignment.<sup>37</sup> Kleptokaryon sequences were distinguished from those of the ciliate host by BLASTp searches<sup>29-31</sup> against a reference database of proteins from the pure culture G. cryophyila transcriptome. Proteins returning hits with E-values  $\leq 1 \times 10^{-50}$  were retained as kleptokaryon-derived.

#### Differential expression analyses

Reads were mapped back to cryptophyte and ciliate transcriptomes by BWA v.0.7.1732 and read counts were extracted for each treatment and replicate with the multiBamCov function from BEDTools v.2.28.033 with gene coordinates obtained from TransDecoder. Differential expression analyses were conducted with the R v.4.0.0 (http://www.R-project.org) package DESeq2.27 Comparisons included high to low light cultures (HL) versus cultures maintained at high light (HH) and low to high light cultures (LH) versus cultures maintained at low light (LL). PCA plots were generated in DESeq2 by first transforming the count data to a log<sub>2</sub> scale with the rlogTransformation function and the experimental design blinded to prevent biased comparisons. The transformed data were then plotted with PCAtools (https://github.com/kevinblighe/PCAtools) in R.<sup>26</sup>

#### **Proteomics**

#### Protein extraction

Proteins were extracted from 47 mm 0.2 µm polycarbonate filters using a modified magnetic bead method from Hughes et al. 38 SP3 method. Filter sections were placed in protein extraction buffer (50 mM HEPES pH 8.5, 1% SDS in HPLC grade water), and samples were heated at 95°C for 10 minutes, shaken at room temperature for 15 minutes, and centrifuged for 30 minutes at 14,100 g (Eppendorf Minispin centrifuge). Supernatant was removed from the pellets and transferred to Vivaspin 5K MWCO ultrafiltration units (Sartorius Stedim), and protein extracts were concentrated, washed with protein extraction buffer (above), and transferred to ethanol washed microtubes.

#### Protein reduction and alkylation

Benzonase nuclease (50 U) was added to each sample and incubated at 37°C for 30 minutes. Samples were reduced by adding 200 mM DTT (in 50mM HEPES, pH 8.5) at 45°C for 30 minutes, then alkylated by adding 400 mM iodoacetamide (in HEPES, pH 8.5) for 30 minutes at 24°C, occasionally heating to 37°C to prevent precipitation. The reaction was guenched by adding 200 mM DTT.

#### Protein clean up

Sera-Meg SpeedBead and Carboxylate Modified Magnetic Particles (GE Healthcare) were prepared by making a 1:1 stock combination, rinsing with water, and storing at 4°C at a concentration of 10 μg/μl until use. 38 To each protein sample, 2 μl of this bead stock was added to extracted protein samples and mixed by pipette to generate a homogeneous solution. The mix was periodically heated to avoid precipitation. Samples were acidified to a pH of 2-3 by adding 10% formic acid, and 2X volume of acetonitrile was immediately added. Samples were then incubated at 37°C for 15 minutes, followed by room temperature for 30 minutes, before being





placed on a magnetic rack and incubated for 2 minutes. Supernatant was then discarded, and samples were briefly washed with 70% ethanol 2 times on the magnetic rack, followed by a wash with acetonitrile, with the supernatant removed and discarded each time. Samples were then air dried just until acetonitrile evaporated, and the beads were removed and reconstituted in 50 mM HEPES (0.8 Hq)

#### **Protein quantification**

Standard curves were generated using an albumin standard, and total protein was quantified using the BCA method (Thermo Scientific Micro BCA Protein Assay Kit). Absorbance was measured on a Nanodrop ND-1000 spectrophotometer (Thermo Scientific). Digestion, Peptide recovery and preparation

Trypsin (0.5μg/μL) dissolved in HEPES (pH 8.0) was added to samples at a 1:25, trypsin to protein ratio and incubated at 37°C overnight. Digested peptide samples were then added to acetonitrile and incubated for 20 minutes at room temperature, before being placed on a magnetic rack for 2 minutes. The supernatant was removed and samples were again washed with acetonitrile on the magnetic rack for 15 seconds. Samples were air dried just until acetonitrile evaporated, and beads were reconstituted in 2% DMSO at room temperature. Samples were then pulse centrifuged (900xg), incubated on the magnetic rack for 15 minutes, and peptides were collected in the supernatant. Trifluoroacetic acid was added (0.1%) and samples were purified with Pierce C18 tips, according to manufacturer's protocol, and evaporated to approximately 10μL in a DNA110 Speedvac (ThermoSavant). Samples were finally resuspended to a peptide concentration of 1µg/µL in buffer B (2% acetonitrile, 01% formic acid).

#### Peptide Sequencing and proteomic analysis

Tryptic peptides were analyzed via liquid chromatography tandem mass spectrometry (LC/MS/MS) using a Michrom Advance HPLC system with reverse phase chromatography coupled to a Thermo Scientific Q-Exactive Orbitrap mass spectrometer with a Michrom Advance CaptiveSpray ionization source. Each sample was concentrated onto a trap column (0.2 x 10 mm ID, 5 µm particle size, 120 Å pore size, C18 Reprosil-Gold, Dr. Maisch GmbH) and rinsed with 100 μL 0.1% formic acid, 2% acetonitrile (ACN), 97.9% water before gradient elution through a reverse phase C18 column (0.1 x 150 mm ID, 3 μm particle size, 120 Å pore size, C18 Reprosil-Gold, Dr. Maisch GmbH) at a flow rate of 500 nL/min. The chromatography consisted of a nonlinear 170 min gradient from 5% to 95% buffer B, where A was 0.1% formic acid in water and B was 0.1% formic acid in acetonitrile. The mass spectrometer monitored MS1 scans from 380 m/z to 1280 m/z at 70K resolution. MS2 scans were performed on the top 15 ions with an isolation window of 2.0 m/z and a 15 second exclusion time. Mass spectra were searched against the translated transcriptomes of Mesodinium rubrum and Geminigera cryophila (from these experiments) using Proteome Discoverer's SEQUEST HT algorithm (Thermo) with a fragment tolerance of 0.02 Da and parent tolerance of 10 ppm. Identification criteria consisted of a protein threshold of 99% and two minimum peptides, corresponding to a protein FDR of 0.7% and peptide FDR of 0.01% when analyzed with Scaffold version 5.1.2 (Proteome Software, Inc.). The mass spectrometry proteomics data have been deposited to the ProteomeXchange Consortium via the PRIDE<sup>39</sup> partner repository with the dataset identifier PXD035728 and 10.6019/PXD035728

#### **Metabolomics**

All metabolomic analyses were conducted by the West Coast Metabolomics Center, at University of California, Davis.

#### Primary metabolism by GC-TOF MS

In this platform, ~150 identified compounds were detected in addition to ~250 unknowns. It includes sugars, TCA metabolites, amino acids, hydroxyl acids such as lactate, free fatty acids, aromatics, polyamines, nucleosides, and monophospho nucleotides. Filters were combined with 1 mL of degassed acetonitrile: isopropanol:water (3:3:2, v/v/v) and metabolites were extracted by homogenization for 5 min on ice. The homogenate was then centrifuged (16,100 rcf, at 4°C), decanted, and evaporated. Extracts were cleaned with 0.5 mL of degassed acetonitrile: water (1:1, v/v) to remove triglycerides and membrane lipids, and then evaporated again. For GC-MS analysis, internal standard C8-C30 fatty acid methyl esters were added to determine the retention index (RI) as follows: 2 μl of the RI mixture were added to the dried extracts that included C8, C9, C10, C12, C14, C16, C18, C20, C22, C24, C26, C28, and C30 linear chain length, dissolved in chloroform at a concentration of 0.8 mg/ml (C8-C16) and 0.4 mg/ml (C18-C30). The dried samples with RI were derivatized with 10 µL of methoxyamine hydrochloride in pyridine and again with 90 µL of MSTFA (or MSTFA-d9) for trimethylsilylation of acidic protons. The extracted samples were resuspended in 50 µL of acetonitrile: water (4:1, v/v) and applied to the instrument for LC-MS analysis. 40,41

#### **Injector conditions**

Agilent 6890 GC was equipped with a Gerstel automatic liner exchange system (ALEX) that includes a multipurpose sample (MPS2) dual rail, and a Gerstel CIS cold injection system (Gerstel, Muehlheim, Germany) with temperature program as follows: 50°C to 275°C final temperature at a rate of 12 °C/s and hold for 3 minutes. Injection volume was 0.5 μl with 10 μl/s injection speed on a splitless injector with purge time of 25 seconds. Liner (Gerstel #011711-010-00) was changed after every 10 samples, (Maestro Gerstel software). Before and after each injection, the 10 μl injection syringe was washed three times with 10 μl ethyl acetate.

#### Gas Chromatography conditions

A 30 m long, 0.25 mm i.d. Rtx-5Sil MS column (0.25 µm 95% dimethyl 5% diphenyl polysiloxane film) with additional 10 m integrated guard column was used (Restek, Bellefonte PA). Pure Helium (99.9999%) with built-in purifier (Airgas, Radnor PA) was set at constant flow of 1 ml/min, and the oven temperature was held constant at 50°C for 1 min and then ramped at 20°C/min to 330°C at which it was held constant for 5 min.

### **Current Biology** Report



#### Mass spectrometer settings

A Leco Pegasus IV time of flight mass spectrometer was controlled by the Leco ChromaTOF software (St. Joseph, MI). The transfer line temperature between gas chromatograph and mass spectrometer was set to 280°C. Electron impact ionization at 70V was employed with an ion source temperature of 250°C. Acquisition rate was 17 spectra/second, with a scan mass range of 85-500 Da.

#### **Lipidomics Sample Preparation**

Extraction of plasma lipids was based on the "Maytash" method<sup>42</sup> which was subsequently modified. Extraction was carried out using a bi-phasic solvent system of cold methanol, methyl tert-butyl ether (MTBE), and water. In more detail, cold methanol (225 μL) containing a mixture of odd chain and deuterated lipid internal standards [lysoPE(17:1), lysoPC(17:0), PC(12:0/13:0), PE(17:0/17:0), PG(17:0/17:0), sphingosine (d17:1),  $d_7$ -cholesterol, SM(17:0), C17 ceramide,  $d_3$ -palmitic acid, MG(17:0/0:0/0:0), DG(18:1/2:0/0:0), DG(12:0/12:0/0:0), and  $d_5$ -TG(17:0/17:1/17:0)] was added to a 20  $\mu$ L sample aliquot, placed into a 1.5 mL micotube, and vortexed for 10 s. Then, 750 μL of cold MTBE containing CE(22:1) (internal standard) were added, followed by vortexing for 10 s, and shaking for 6 min at 4°C. Phase separation was induced by adding 188 µL of mass spec-grade water. After vortexing for 20 s, the sample was centrifuged at 14,000 rpm for 2 min. The upper organic phase was collected in two 300 μL aliquots. One was stored at -20°C as a backup and the other was evaporated to dryness in a SpeedVac. Dried extracts were resuspended using a mixture of methanol/toluene (9:1, v/v) (60 μL) containing an internal standard [12- [[(cyclohexylamino)carbonyl]amino]- dodecanoic acid (CUDA)] used as a quality control.

#### LC/MS parameters

The LC/QTOFMS analyses were performed using an Agilent 1290 Infinity LC system (G4220A binary pump, G4226A autosampler, and G1316C Column Thermostat) coupled to either an Agilent 6530 (positive ion mode) or an Agilent 6550 mass spectrometer equipped with an ion funnel (iFunnel) (negative ion mode). Lipids were separated on an Acquity UPLC CSH C18 column (100 x 2.1 mm; 1.7 μm) maintained at 65°C at a flow-rate of 0.6 mL/min. Solvent pre-heating (Agilent G1316) was used. The mobile phases consist of 60:40 acetonitrile:water with 10 mM ammonium formate and 0.1% formic acid (A) and 90:10 propan-2-ol:acetonitrile with 10 mM ammonium formate and 0.1% formic acid. The gradient was as follows: 0 min 85% (A); 0-2 min 70% (A); 2-2.5 min 52% (A); 2.5-11 min 18% (A); 11-11.5 min 1% (A); 11.5-12 min 1% (A); 12-12.1 min 85% (A); 12.1-15 min 85% (A). A sample volume of 3 µL was used for the injection, and sample temperature was maintained at 4°C in the autosampler.

The quadrupole/time-of-flight (QTOF) mass spectrometers are operated with electrospray ionization (ESI) performing full scan in the mass range m/z 65-1700 in positive (Agilent 6530, equipped with a JetStreamSource) and negative (Agilent 6550, equipped with a dual JetStream Source) modes producing both unique and complementary spectra. Instrument parameters were as follows (positive mode) Gas Temp 325°C, Gas Flow 8 I/min, Nebulizer 35 psig, Sheath Gas 350°C, Sheath Gas Flow 11, Capillary Voltage 3500 V, Nozzle Voltage 1000V, Fragmentor 120V, Skimmer 65V. Data (both profile and centroid) are collected at a rate of 2 scans per second. In negative ion mode, Gas Temp 200°C, Gas Flow 14 I/min, Fragmentor 175V, with the other parameters identical to positive ion mode. For the 6530 QTOF, a reference solution generating ions of 121.050 and 922.007 m/z in positive mode and 119.036 and 966.0007 m/z in negative mode, were used for continuous mass correction. For the 6550, the reference solution was introduced via a dual spray ESI, with the same ions and continuous mass correction.

Samples were injected (1.7 μl in positive mode and 5 μl in negative ion mode) with a needle wash for 20 seconds (isopropanol wash solvent). The valve was switched back and forth during the run for washing, which has been shown to be critical for reducing carryover of less polar lipids.

#### **Data Analysis**

For the data processing the MassHunter software was used, and a unique ID was given to each lipid based on its retention time and exact mass (RT\_mz). This allows the report of peak areas/heights or concentration of lipids based on the use of particular internal standards. Lipids were identified based on their unique MS/MS fragmentation patterns using in-house software, Lipidblast.<sup>34</sup> Using complex lipid class-specific internal standards this approach was used to quantify >400 lipid species including: mono-, di- and triacylglycerols, glycerophospholipids, sphingolipids, cholesterol esters, ceramides, and fatty acids. This highly reproducible approach displays a relative standard deviation of 0.1% for the retention time and 1.7% for peak area based on replicate analysis of plasma samples (n=10). An average shot-to-shot carryover of less than 0.1% is generally observed.

#### **QUANTIFICATION AND STATISTICAL ANALYSIS**

All cell count, Fv/Fm, and pigment data were subjected to tests for normality and homoscedasticity using a Shapiro-Wilk test and by creating Q-Q plots in R using the packages dplyr (1.0.7), ggpubr (0.4.0), and qqplotr (0.0.5). Data that did not meet the requirements of a normal distribution were log transformed and re-tested. All normally distributed data were analyzed by parametric statistical tests, including T-Tests and one- and two-way ANOVAs with post-hoc testing of treatment means using Tukey HSD tests in R using gplots (3.1.1) and ggplot2 (3.3.5). Non-parametric analysis of data was achieved using the Kruskal-Wallis rank sum test with the R packages lattice (0.20-45), rcompanion (2.4.6), coin (1.4-2), and FSA (0.9.1). All analyses in R were run using version 4.1.1.<sup>20</sup>